Dusty plasmas: Experiments on nonlinear dust acoustic waves, shocks, and structures

R. L. Merlino, J. R. Heinrich,[1] S-H. Kim, and J. K. Meyer

Department of Physics and Astronomy

The University of Iowa, Iowa City, IA, 53342 USA

Email: robert-merlino@uiowa.edu

Submitted to Plasma Physics and Controlled Fusion, June 27, 2012

Special Issue: 2012 EPS/ICPP

PACS numbers: 52.27.Lw, 52.35.Tc, 52.35.Fp

Short Title: dust acoustic waves, shocks, and structures

Abstract.

A review is presented of recent experiments performed on the University of Iowa DC discharge dusty plasma device on various aspects of dust acoustic waves. A brief introduction to the physics of dusty plasmas and the dust acoustic wave is first presented. Three experiments are then described: (i) observation and interpretation of large amplitude (nonlinear) dust acoustic waves; (ii) evolution of large amplitude dust acoustic waves into shocks, and comparison to numerical shock solutions of the generalized hydrodynamic equations; and (iii) the spontaneous formation of stationary, stable dust structures in a moderately coupled dusty plasma (dust structurization).

[1] Present address: Air Force Research Laboratory, Kirtland AFB, NM

Outline

1. Introduction

A dusty (complex) plasma is a multicomponent system consisting of electrons, ions, charged mesoscopic particles (dust grains), and neutral atoms or molecules [1,2]. Interest in this ‘unusual’ state of matter stems from the ubiquity with which it is found in the laboratory, in space, and in astrophysics, such as: cometary tails, planetary rings, solar and planetary nebulae, the lower ionosphere (mesosphere), atmospheric lighting, and industrial plasma processing and nanomaterials fabrication devices [3]. In this introduction, we first provide some of the background ‘basics’ of dusty plasma physics, concentrating of the differences compared to non-

dusty plasmas, followed by a summary of the physics of the fundamental wave mode of a dusty plasma — the dust acoustic wave [4], which is the phenomenon underlying the topics of this paper.

1.1 Dusty plasma basics

In typical laboratory experiments, a dust particle acquires an electric charge by collecting electrons and ions from the plasma [5]. Since the speed of the electrons is typically much larger than that of the positive ions, the dust grain first collects electrons and charges to a negative potential, relative to the plasma, which impedes further electron collection and enhances ion collection. The net result is that the dust grain will have a negative charge. The surface potential (V_s) of the dust grain relative to the plasma is determined by the (floating) condition that in equilibrium the net current to the grain must be zero. The equilibrium charge on the dust grain, Q_d, is then computed by treating it as an isolated spherical conductor of capacitance $C_d = 4\pi\varepsilon_o a$, where a is the radius of the grain, using $Q_d = C_d V_s$. A useful rule of thumb for an isolated dust grain of radius a_μ in microns, in a singly-ionized argon plasma having electron and ion temperatures, $T_e = 100T_i = 2.5$ eV, is $Q_d \approx -4000ea_\mu$, where e is the electronic charge. Thus, a dust grain of 1 μm diameter will have a charge, $Q_d \approx -2000e$. If the dust grain is composed of material of mass density 2000 kg/m^3, it's mass is, $m_d \sim 10^{-15}$ kg ($m_d/m_p \sim 5\times10^{11}$), so that it's charge to mass ratio is $(Q_d/m_d) \sim 0.3$ C/kg $<< (e/m_p)$, where m_p is the proton mass. The relatively low value of the charge to mass ratio of the dust grain plays an important role in determining its dynamical behavior in electric and magnetic fields.

The size, mass, and charge of a typical micron-size dust grain in a laboratory plasma makes it susceptible to forces that are not usually important for non-dusty plasmas, such as the weight of the grain, $m_d g$. Due to their non-negligible weight, dust grains must be levitated so they don't fall out of the plasma. Electrostatic fields usually provide the levitation force, as well as horizontal forces that confine the dust grains. For example, a dust grain of 1 micron diameter requires a modest levitation electric field $E = m_d g/Q_d \sim 30$ V/m. Thermophoretic forces [5] have also been used to levitate dust grains.

Another important force on dust grains is the ion drag force [5]. This is the force exerted on a dust grain due to its interaction with drifting ions. A dust grain absorbs momentum not only from ions that directly impact it, but also by ions making Coulomb collisions with it. The ion drag

force is responsible for the formation of “voids” in dusty plasmas, regions where dust grains have been pushed out. Voids were first observed in dusty plasmas in the microgravity environment of the International Space Station [6].

1.2 Physics of the dust acoustic wave

The dust acoustic (DA) wave is a low frequency, longitudinal wave characterized by propagating dust density compressions and rarefactions [4]. It is a sound wave propagating through the charged dust fluid, involving oscillations of the heavy dust grains. The interactions between the charged dust grains are mediated by the collective electric fields in the plasma. The existence of the DA wave was suggested almost 25 years ago by Padma Shukla at the First Capri Workshop on Dusty Plasmas in 1989. The detailed analysis of this dust wave was worked out by Rao, Shukla and Yu a few months later [4]. Shukla’s contribution was in treating the dust as a separate fluid component which could support electrostatic waves of such a low frequency that the inertia of both the electrons *and* ions could be ignored (Boltzmann response). An intriguing aspect of the dust acoustic wave is that, due to light scattering from the grains, the waves could be seen propagating through the dust suspension with the naked eye [7].

The physics of the dust acoustic wave can be understood in its simplest form by assuming that the dust kinetic temperature is zero, so that the momentum equation for the dust in one-dimension is

$$m_d n_d \left(\frac{\partial v_d}{\partial t} + v_d \frac{\partial v_d}{\partial x} \right) = e Z_d n_d \frac{\partial \varphi}{\partial x}. \qquad (1)$$

Here, m_d, n_d, Z_d and v_d are, respectively, the dust mass, number density, charge number and fluid velocity, and φ is the electric potential, which is related to the ion, electron and dust charge densities through Poisson’s equation

$$\frac{\partial^2 \varphi}{\partial x^2} = -\frac{e}{\varepsilon_o}\left(n_i - n_e - Z_d n_d \right), \qquad (2)$$

where n_i and n_e are the ion and electron number densities. The momentum equations for the ions and electrons, with temperatures T_i and T_e, and with $m_e = m_i = 0$, are

$$0 = -\frac{\partial p_i}{\partial x} - en_i \frac{\partial \varphi}{\partial x}, \tag{3a}$$

$$0 = -\frac{\partial p_e}{\partial x} + en_e \frac{\partial \varphi}{\partial x}, \tag{3b}$$

where $p_e = n_e k_B T_e$ and $p_i = n_i k_B T_i$ are the electron and ion pressures. For long wavelengths, Poisson's equation (3) is replaced by the quasineutrality condition

$$n_i - n_e - Z_d n_d = 0. \tag{4}$$

Equation (4) can be combined with (3a) and (3b) to relate the electric potential to the gradient in the ion and electron pressure as

$$\frac{\partial \left(p_i + p_e \right)}{\partial x} = \frac{\partial p}{\partial x} = -eZ_d n_d \frac{\partial \varphi}{\partial x}, \tag{5}$$

where $p = p_e + p_i$ is the total plasma pressure. Equation (5) is used to write the electric field in (1) in terms of the plasma pressure, and together with the continuity equation, we have the following set of equations for the dust acoustic wave

$$\frac{\partial v_d}{\partial t} = -\left(\frac{1}{\rho_d} \frac{\partial p}{\partial x} + v_d \frac{\partial v_d}{\partial x} \right), \tag{6a}$$

$$\frac{\partial \rho_d}{\partial t} = -\left(\rho_d \frac{\partial v_d}{\partial x} + v_d \frac{\partial \rho_d}{\partial x} \right), \tag{6b}$$

where $\rho_d = m_d n_d$ is the dust mass density. From (6a) we see that in the dust acoustic wave, the oscillations involve the dust inertia and a restoring force provided by the plasma pressures. We note also that (6a) and (6b), which are nonlinear equations, are identical to the Euler equations for an invicid fluid. We can then expect that these equations would predict the existence of dust

acoustic shock waves, just as the Euler equations have been shown to predict shocks in a neutral gas.

The dispersion relation for the dust acoustic wave is obtained by linearization of (1) through (6). Equations (4) and (5) are linearized and combined to relate the dust acoustic wave potential, $\varphi_{1,}$ to the first order dust density, $n_{d1,}$ as

$$\varphi_1 = -\left(\frac{eZ_d\lambda_D^2}{\varepsilon_o}\right)n_{d1}, \tag{7}$$

where $\lambda_D = \lambda_{Di}\Big/\sqrt{1+\left(\lambda_{Di}/\lambda_{De}\right)^2}$ is the linearized Debye length with $\lambda_{Dj} = \left(\varepsilon_o k_B T_j \big/ e^2 n_j\right)^{1/2}$. The dust momentum and continuity equations (6a) and (6b) are linearized about a homogeneous and time-independent zero-order state with no dust flows, v_{d0} = 0, or electric fields $E_0 = -\dfrac{\partial\varphi_0}{\partial x} = 0$. When the linearized dust momentum and continuity equations are combined with (7) we obtain, by elementary calculation, a wave equation for n_{d1}

$$\frac{\partial^2 n_{d1}}{\partial x^2} = \frac{1}{\omega_{pd}^2\lambda_D^2}\frac{\partial^2 n_{d1}}{\partial t^2} \tag{8}$$

which provides the dispersion relation for non-dispersive dust acoustic waves

$$\frac{\omega}{k} = C_{da} = \omega_{pd}\lambda_D \approx \sqrt{\frac{n_{d0}}{n_{i0}}\frac{Z_d^2 k_B T_i}{m_d}}, \tag{9}$$

where $\omega_{pd} = \left(e^2 Z_d^2 n_{d0}/\varepsilon_o m_d\right)^{1/2}$ is the dust plasma frequency, ω and k are the wave angular frequency and wavenumber, and n_{i0} is the zero-order ion density. The expression (under the radical) in (9) for the dust acoustic speed is approximate, since for typical laboratory dusty plasmas where $T_e >> T_i$, we used $\lambda_D \approx \lambda_{Di}$ as the plasma shielding length. If finite dust temperatures, T_d, were taken into account, an additional term $k_B T_d / m_d$ would be added to the term under the radical in (9).

Next we consider the question of excitation of the dust acoustic wave. Dust acoustic waves have been observed frequently in dusty plasmas formed in DC and RF glow discharge devices. This is due to the fact that the dust acoustic wave is spontaneously excited by an ion-dust streaming instability [8]. Typical discharge plasmas contain drifting ions of sufficient speed for the instability to develop. The fluid theory of the dust acoustic wave has been modified to include collisions between the dust grains and neutrals, ion and electron neutral collisions, and a zero-order electric field that drives the ion drift [9]. As an illustration of the ion-dust streaming instability, Fig. 1 shows results from a numerical solution to the modified dispersion relation which takes into account the ion drift. In Fig. 1(a) the real and imaginary parts of the wave frequency are shown as a function of the ion drift speed relative to the ion thermal speed. It is seen that for a typical set of parameters relevant to laboratory dusty plasmas, that instability develops, $\omega_i > 0$, for relatively modest ion drifts, v_{id}, with $v_{id} / v_{it} \sim 1$, where v_{it} is the ion thermal speed. Fig. 1(b) shows that at high gas pressures, dust neutral collisions can quench the wave. As we will see later in this paper, the dust acoustic wave is quite robust, and typically reaches high amplitudes with nonlinear characteristics. Observation of linear dust acoustic waves requires operation of the dusty plasma at high neutral pressures where the wave is heavily damped [10], or special experimental configurations that allow the wave to be observed in the very early stages of the linear growth phase [11].

2. A DC glow discharge dusty plasma device

2.1 Plasma production

All of the experiments described in this paper were performed in the device shown schematically in Fig. 2. The device produced a DC glow discharge plasma in a large (60 cm diameter, 90 cm length) stainless-steel vacuum chamber. A 3.2 cm diameter disk, located on the axis of the device with its normal parallel to the axis, served as the anode for the gas discharge, while the grounded chamber walls served as the cathode. The evacuated chamber was filled with argon gas at pressures ~ 100—200 mtorr (13—26 Pa), and a DC potential ~ 250 – 400 V was applied to the anode to produce a discharge, with resulting discharge currents in the range of a few to tens of mA (depending on the pressure and discharge voltage). A double Langmuir probe was used to measure the ion density (n_i) and electron temperature (T_e) , with $n_i \sim 10^{14} – 10^{15}$ m^{-3}, and $T_e \sim 2 – 3$ eV. The ion temperature was assumed to be equal to the temperature of the neutral

gas, ~ 300 K. A magnetic field, typically, 0.003 T, directed along the axis of the device was applied to provide confinement for the electrons and to produce a relatively stable, axially extended, cylindrical plasma with a diameter close to that of the anode. The electric potential contours within the anode glow plasma contains both axial and radial electric field components ~ 100 –500 V/m [12]. A list of the plasma parameters are collected in Table 1.

2.2 Getting dust into a plasma

Although dust is ubiquitous in space and astrophysical plasmas, it must be put into laboratory plasmas in order to study it. One technique is to grow dust in the plasma. By incorporating chemically reactive gases into a plasma, plasma assisted chemical reactions occur which result in the formation of nanometer size dust. These then coagulate and coalesce into larger grains of micron size [13]. Typical ingredients for growing silica grains are argon, oxygen and silane. Methane plasmas have been used to grow carbon dust. Although these methods work very well, the size of the grains depends on how long the process proceeds. Since most theoretical work in dusty plasmas has been done assuming the dust is spherical and all the same diameter, it makes experiment/theory comparisons easier if spherical monodisperse dust is used; however, it is not necessary to use monodisperse grains to form a dusty plasma. On the other hand, since space/astrophysical dusts are not likely to be spherical and monodisperse, experiments should be performed to investigate dusty plasmas having grains with various sizes and shapes [14]. The theoretical analysis of dusty plasmas with polydisperse grains becomes quite complicated, however, due to the distribution of grain charges and masses.

In our experiments, commercially fabricated dust grains of known sizes were used. The dust grains were placed on a floating horizontal metal tray located a few centimeters below the anode. Roughly a few hundred grams of dust was spread on the tray. The dust was incorporated into the plasma when the discharge was ignited. The process requires some finesse on the part of the operator in making adjustments to the discharge current, gas pressure, and magnetic field until a well-formed stable suspension is achieved. The dust incorporation and trapping process has not been studied in detail, nor has any theoretical modeling been done. Present thinking is that the dust on the top of the pile becomes charged by the plasma during the discharge start-up and lifted up into the main plasma volume. The dust is confined within the anode glow by a combination of electric forces arising from the potential structure of the anode glow, and ion drag forces [15].

The trapping of dust in the plasma is a self-regulating process— the plasma seems to limit the amount of dust that it can confine, and once this limit is reached, the trapping process ends, with no further indication of more dust being lifted into the plasma. The process lasts on the order of a few minutes, after which a relatively stable dust cloud is formed. Interestingly, a similar process is thought to lift dust off of the lunar regolith [16].

The dust suspension is imaged using 532 nm light from a diode laser that is expanded using a cylindrical lens into a thin (~ mm thickness) sheet which illuminates a thin slice of the cloud. The light scattered from the dust is imaged using a CMOS video camera (Photron Fastcam 1024 PCI) with a megapixel active area. Typically, the dust behavior is recorded at up to 1000 frames per second. The camera has a linear response to light intensity, so that the image intensity is directly proportional to the dust density. The dust parameters are listed in Table 1.

2.3 Interactions between dust grains in a DC glow discharge dusty plasma

As mentioned previously, a dusty plasma is an unusual state of matter. This is due, in part, to the fact that the interactions between the dust grains (dust-dust) are relatively strong, while interactions between electrons and electrons, ions and ions, and electrons and ions are relatively weak. We say that the dust component is 'strongly coupled' while the plasma component is 'weakly coupled'. The degree of strong coupling of the dusty plasma dictates the type of theoretical analysis that is required to model its behavior. The coupling parameter, Γ, the ratio of potential energy due to dust-dust interactions to the dust kinetic energy, is used to quantify the degree of interaction, and it is instructive to estimate its value for the typical laboratory dusty plasmas that are being discussed in this paper. The dust coupling parameter is given by

$$\Gamma = \frac{1}{4\pi\varepsilon_o}\frac{Q_d^2\, e^{-\kappa}}{\Delta\; k_B T_d} \qquad [10]$$

where $\Delta = \left[3/\left(4\pi n_d\right)\right]^{1/3}$ is the average interparticle spacing, $\kappa = \Delta/\lambda_{Di}$, and the exponential term takes into account Debye shielding of the dust grains [17]. For typical values of the plasma parameters (see Table 1) we find that $\Gamma_e, \Gamma_i << 1$; the plasma is weakly coupled and behaves like a gas of charged particles. For typical dust parameters, a = 0.5 μm, Q_d ~ –2000e, and n_d ~ 5×10^{10} m^{-3}, we find that $\Gamma \approx \left(10\text{ eV}\right)/T_{d,eV}$, where $T_{d,eV}$ is the dust temperature in eV. The dust

temperature is not an easy parameter to measure, but we can make the following observations. If the dust is cold (in thermal equilibrium with the neutral gas), T_d = 0.03 eV, then $\Gamma_d \approx 300 >> 1$; the dust would be strongly coupled. For 'hot" dust with T_d = 10 eV, $\Gamma \sim 1$, while for 'very hot' dust, T_d = 100 eV, $\Gamma \sim 0.1$. From observations of the dust clouds in our experiments, it appears that the dust is not in the strongly coupled state in which the grains would be locked into a crystalline lattice. It is then unlikely that the dust is either in the strongly coupled ($\Gamma >>1$) or weakly coupled ($\Gamma <<1$) state, and more likely to be in the moderately coupled, liquid state, with $\Gamma \sim 1$.

3. Nonlinear dust acoustic waves

3.1 Experimental observations

A concise review of the basic theoretical and experimental work on the dust acoustic wave is contained in the introduction to ref. 18. The dust acoustic waves were observed in the device shown in Fig. 2. The waves appeared spontaneously when the dust suspension was formed. The intensity of the light scattered from the dust (proportional to the dust density) was recorded with the video camera, and a single frame image from the video is shown in Fig. 3(a), where the wave fronts are seen as the bright vertical bands. The waves propagated from left to right in this image. The intensity of the scattered light within the rectangle in Fig. 3(a) is shown in Fig. 3(b) (filled circles). In Fig. 3(b) the average dust density, $\langle n_d \rangle$, taken over a long video recording has been subtracted from the measured intensities to obtain the actual waveform of the dust acoustic wave. The wave amplitudes, $\Delta n_d / \langle n_d \rangle$ corresponding to the three wave crests at 2 mm, 6.5 mm, and 11 mm in Fig. 3(b) are respectively, 0.66, 0.85, and 1.0. The nonlinear dust acoustic waves have non-sinusoidal waveforms, with peaked wave crests and flat wave troughs. The wave phase speed was $v_{ph} \approx 28$ cm/s, as measured by following one wavefront in time, as shown in Fig. 3(c). The wave frequency was also obtained from the video and found to be 54 Hz, which together with the measured wave speed, yields a wavelength ~ 5 mm, which is consistent with the wavelength determined directly from the waveform shown in Fig. 3(b).

It is of interest to compare the measured wave speed with estimates of the dust acoustic speed. If the thermal speed of the dust is included in the dust acoustic speed (9), then $C_{da} = \left(v_{d,t}^2 + \lambda_{Di}^2 \omega_{pd}^2 \right)^{1/2}$, where $v_{d,t} = \left(kT_d / m_d \right)^{1/2}$ is the dust thermal speed. As remarked earlier,

the dust temperature was not measured; however, if reasonable estimates for the plasma and dust parameters are used, we find that the largest expected value for C_{da} is about l5 cm/s. The inequality $v_{ph} > C_{da}$, is a further indication that the waves were nonlinear.

3.2 Discussion: second order dust acoustic wave theory

The non-sinusoidal dust acoustic waveforms shown in Fig. 3(b) cannot be explained using linear theory. The simplest approach is to start with the continuity and momentum equations for the dust fluid, and expand all the relevant quantities to second order [19], to obtain a nonlinear dust acoustic wave equation for the second order dust density, n_{d2}

$$\frac{\partial^2 n_{d2}}{\partial x^2} - \frac{1}{C_{da}^2}\frac{\partial^2 n_{d2}}{\partial t^2} = A\frac{\partial^2 n_{d1}^2}{\partial x^2} + B\frac{\partial^2 n_{d1}^2}{\partial x \partial t}, \qquad [11]$$

where, $A = A_2/A_1 - \omega^2\Big/\left(2k^2 n_{d0} C_{da}^2\right)$, $B = \omega\Big/\left(2k^2 n_{d0} C_{da}^2\right)$, with $A_1 = -eZ_d\lambda_D^2/\varepsilon_o$,

$A_2 = e^3 Z_d^2 \lambda_D^6\left(1-\alpha\tau^2\right)\Big/\left(2\varepsilon_o^2 kT_i\lambda_{Di}^2\right)$, $\alpha = n_{e0}/n_{i0}$, and $\tau = T_i/T_e$. Equation (11) is an inhomogeneous wave equation with source terms (RHS) that involve products of first order terms. For plane wave solutions, the first order dust density is, $n_{d1} \sim \exp\left[i\left(kx-\omega t\right)\right]$, so the source terms in (11) produce second harmonic waves of the form $n_{d2} \sim \exp\left[2i\left(kx-\omega t\right)\right]$. The solution to (11) for the dust density is then $n_d = n_{d0} + n_{d1} + n_{d2}$, so that dust density perturbation $\Delta n_d = n_d - n_{d0}$ at an arbitrary time (t = 0) can be written

$$\Delta n_d(x,0) = \tilde{n}_{d1}\cos\left(kx-\omega t\right) + \tilde{n}_{d2}\cos\left[2\left(kx-\omega t\right)\right] \qquad [12]$$

where $\tilde{n}_{d1}$ and $\tilde{n}_{d2}$ are the first and second order amplitudes. Equation (12) was applied to the waveform in Fig. 3(b) (full red curve) using the measured wavelength, with $\tilde{n}_{d1}$ and $\tilde{n}_{d2}$ chosen to give the best fit. The best fit to the data required that the second harmonic term was approximately 30% of the first harmonic term. The addition of the second harmonic term gives a waveform with sharp peaks and flat troughs that is more representative of the measured waveform.

It is interesting to point out that the paper of Rao, Shukla, and Yu [4], which first predicted the existence of the (linear) dust acoustic wave, also contained the first nonlinear theory of finite

amplitude dust acoustic waves, apparently anticipating the experimental observations of large amplitude dust density waves.

4. Dust acoustic shock waves

Shock waves form due to the steepening of large amplitude compressional waves. The formation of steady-state shocks requires dissipation, such as viscosity, to balance the tendency to steepen. As pointed out in Sec. 1.2, the fluid equations describing nonlinear dust acoustic perturbations are mathematically equivalent to the Euler equations for a neutral gas. (If viscosity were included, the dust fluid equations would then be identical to the Navier-Stokes equations.) Since shocks occur in a gas, e. g., in a shock tube, it is reasonable to expect that shocks would form in a dusty plasma. This was first pointed out by David Montgomery for ion acoustic waves [20]. A dusty plasma affords the possibility of exploring shock dynamics in detail due to the ability to diagnose the dust grains at the single particle level. Apart from the inherent interest in shocks, they are of importance in astrophysical processes in the interstellar medium [21]. It has been suggested out that a dust acoustic shock propagating through a dust molecular cloud could trigger the condensation of dust leading to gravitational collapse [22]. Shock wave propagation in a dusty plasma under microgravity was studied by Samsonov et al. [23].

4.1 Experiment

Dust acoustic shock waves were studied in the device shown in Fig. 2, with one modification. A 1 cm wide horizontal slit was placed a few centimeters in front of the anode. The slit was parallel to the anode and centered on the axis of the anode. The lateral extent of the slit was larger than the diameter of the anode. The slit was electrically floating, so the negative dust grains were excluded from its vicinity, producing a configuration of converging/diverging electric potential contours. A single frame video image of the dust cloud with the slit present is shown in Fig. 4. Dust acoustic waves were spontaneously excited on the anode side of the slit, and were focused by the converging/diverging potentials to a smaller volume as they passed through the slit. This additional compression strengthened the waves, which then evolved into cylindrical shock waves as they propagated away from the slit. Spatial profiles of a dust acoustic shock wave taken along the axis at various times are shown in Fig. 5(a). The pulse labeled as T = 0, (time normalized by ω_{pd}) corresponds to an arbitrary time after it emerged from the slit. The

shock steepened as it propagated, forming a classic saw tooth-like wave that is well-known from gas dynamics [24]. The shock thickness decreased as the shock evolved, and reached a minimum value of about 0.3 mm, which was on the order of the interparticle spacing. Further details of the experiment are given in [25].

4.2 Discussion: theory of dust acoustic shock waves

A fully nonlinear theory of arbitrary-amplitude dust acoustic shock waves has been recently developed by Shukla and Eliasson [26]. The theory employs a generalized hydrodynamic model applicable to dusty plasmas of arbitrary coupling strength. The theory includes effects of dust-dust correlations, shear and bulk viscosities, dust-neutral collisions, and the polarization force caused by ions around the dust grains. Time-dependent numerical solutions of the nonlinear equations for parameters corresponding to those of Fig. 5(a) are shown in Fig. 5(b). The theoretical profiles of the dust density compare favorably with the experimental profiles. In particular, the model reproduced closely the shock speed and amplitude; with a Mach number $M \approx 1.33$. The shock thicknesses in the model were somewhat larger than the experimental shock thicknesses. The shock thickness depends of the viscosity which in turn depends on the coupling parameter, Γ. It might be possible to use the measurements of the shock thickness together with the numerical calculations to obtain more accurate values of the viscosity of a dusty plasma and to study how it varies with Γ.

The dust density profile labeled T = 0 in Fig. 5(a) corresponds to an arbitrarily chosen time after the disturbance passed through the slit. Since this disturbance already had some time to steepen, it does not correspond exactly to the numerical profile at T = 0 [Fig. 5(b)] which was taken to be a Gaussian form. We tried to account for this difference by normalizing the numerical values of the shock amplitude and thickness to the experimental results. This procedure allows us to compare the scaling of the parameters with time. The result, presented in Fig. 6 shows a reasonable agreement of the time evolution of the shock amplitude and thickness.

Finally, we point out that the effect of strong correlations is not the only mechanism that has been considered to provide the dissipation necessary to from a stationary shock. The charge on a dust grain in a plasma may fluctuate due to wave motion which causes oscillations in the plasma currents. The coupling of fluctuating electrostatic fields and dust grains can lead to wave

damping under certain conditions [27]. Dissipation related to the dust charge variation may play a role in the evolution of dust acoustic shocks.

5. Structure formation in a dusty plasma

To maintain a dusty plasma, electrons and ions that are collected by the grains must be replenished by an ionization source, rendering dusty plasmas inherently open systems. Such open, dissipative systems are known to exhibit self-organization and structure formation [28]. Structure formation in dusty plasmas was first discussed theoretically by Morfill and Tsytovich in terms of an ionization instability [29]. The structure formation phenomenon of their theory is qualitatively similar to those of a Jeans instability for dusty plasmas, described by Pandey et al. [30], which may be responsible for large scale cosmic structure formation.

Here we summarize laboratory observations of spontaneous dust structure formation observed in the dc glow discharge dusty plasma; further details are presented elsewhere [31].

5.1 Experimental observations

The experiments were performed in the device shown in Fig. 2. The experiments described here used spherical iron dust grains in the range of 1-4 μm diameter, although the same phenomena was also observed using kaolin powder and hollow glass microspheres. The observations of dust structurization were made in dusty plasmas with higher plasma densities than those used in the experiments described in Sec. 3 and 4. Higher plasma densities were obtained by operating the plasma at higher discharge currents. This change had an unexpected and profound effect on the dust cloud configuration.

When the discharge current was < 10 mA, propagating dust acoustic waves were observed. When the discharge current was increased above 16 mA, the dust cloud split into a primary cloud of high dust density close to the anode, and a secondary longer cloud of much lower dust density located farther from the anode. Dust density structures, regions of high dust density separated by regions of low dust density, appeared in the secondary could. A single frame image of the structured dust cloud is shown in Fig. 7(a). In this image, the anode is on the right side, the denser (bright) primary cloud is just to the left of the anode, and the structured secondary cloud is to the left of the primary cloud. This image was taken using a 2 mm wide vertical sheet of laser light (532 nm) that passed through the center of the cloud. The structures were stationary

and stable as shown in Fig. 7(b), where 10 light intensity profiles, taken across the dashed line in Fig. 7(a) over a 33 s interval are overlaid. Multiple images of the structured cloud were taken by positioning the laser sheet through a series of cross-sectional slices. These images were used to produce a tomographic reconstruction of the cloud as shown in Fig. 8. The cloud appeared as a series of nested conical or helical structures. The spatial periodicity (wavelength) of the structures varied with the plasma density (the wavelength decreased from ~ 5 mm at a plasma density of ~ 2×10^{14} m^{-3} to ~ 2 mm at a density 4×10^{14} m^{-3}), as well as the neutral gas pressure (at a constant plasma density of 3×10^{14} m^{-3} the wavelength decreased from ~ 4 mm at 120 mtorr to ~ 2.5 mm at 185 torr).

Since glow discharges are sometimes striated, we checked to see if the structurization of the dust was related to potential structures that might be present in the plasma before the dust was added. With the dust removed, an emissive probe was used to measure the plasma potential along the axis of the anode. There was no evidence of striations or potential structures in the plasma; the potential decreased monotonically with distance from the anode. It appeared that the structurization was due to an intrinsic self-organization process occurring in the dusty plasma, as predicted by Morfill and Tsytovich [29.

5.2 Discussion: ionization instability, ion drag and polarization forces

Stationary dust structures were observed in the dc discharge dusty plasma when the discharge current (~ plasma density) was increased above a critical value. Below the critical discharge current, propagating dust acoustic waves were present, thus it is reasonable to hypothesize that the dust acoustic waves were precursors of the non-propagating dust density structures. There are two theoretical mechanisms that have been shown to produce growing, zero-frequency (non-propagating) dust acoustic-like perturbations in a dusty plasma: (a) ionization instability with the ion drag force [32], and (b) the polarization force [33]. We will discuss each of these separately.

5.2.1 *Ionization and ion drag force*

D'Angelo [32] included the effects of ionization and the ion drag force in a linear instability analysis of dust acoustic waves. He found that the dust acoustic waves were increasingly damped as the effect of the ion drag force increased up to some critical value of the drag coefficient. However, when the ion drag was increased above this critical value, there was a transition from a

propagating dust acoustic wave to a non-propagating zero frequency growing perturbation. The appearance of a stationary perturbation was explained (see Fig. 7 of ref. 32) by the fact that in a dust acoustic wave the electron density perturbation is in phase with the potential perturbation, whereas the ion and dust density perturbations are both out of phase with it. If a spontaneous perturbation causes the dust density to decrease in some region, the potential in that region and the electron density increase. Since the ionization rate depends upon the electron density, this causes the plasma density in the region to increase further. Due to the higher potential, the newly formed ions move out of this region, causing additional outward drag on the dust, thus resulting in instability.

5.2.2 *Effect of the polarization force*

The effect of the polarization force on dust acoustic waves was analyzed by Khrapak et al. [33]. The total force acting on a dust grain in a non-uniform plasma in an external electric field $\vec{E}$ is $\vec{F}_e = Q_d\vec{E} - Q_d^2\nabla\lambda_D\big/\left(2\varepsilon_o\lambda_D^2\right),$ where λ_D is the linearized Debye length defined earlier [34]. The first term is the usual electric force while the second term is due to plasma polarization around the grain. In electron-ion plasmas, the second term is usually negligible, but in a dusty plasma this term can be significant due to the large dust charge. Khrapak et al [33] included the polarization force term in the fluid momentum equation for the dust grains, and derived a modified dust acoustic dispersion relation, which in the long wavelength limit can be written as $\omega/k = \omega_{pd}\lambda_D\sqrt{1-\Re}$, where $\Re = \beta_T/4,$ is factor that is the result of taking the polarization force into account, and $\beta_T = \rho_o/\lambda_D$, is the ratio of the Coulomb radius of interaction between thermal ions and the grain and the linearized Debye length, with $\rho_o = eQ_d\big/\left(4\pi\varepsilon_o k_B T_i\right)$. When $\Re > 1,$ the modified dispersion relation predicts a transition from propagating dust acoustic waves to non-propagating growing perturbations.

Note that both models were based on the linearized fluid equations, so neither can predict what the final state of the respective processes would be. The structurization instability discussed by Morfill and Tsytovich [29], includes the effects of ionization and ion drag forces as well as dust charge variation, but does not include the polarization force. Detailed comparisons of the results of both models (a) and (b) with the experiment were discussed in [31].

6. Summary and concluding remarks

This paper has presented a review of recent experiments performed on the University of Iowa DC discharge dusty plasma device. The experiments discussed here had in common the spontaneous excitation of low-frequency dust acoustic waves. The experiments were performed with dust in the "moderately coupled," $\Gamma \sim 1$ state, which is usually referred to as the liquid state.

The major findings of these experiments are summarized as follows:

(1) Large amplitude (non-linear) dust acoustic waves were typically observed in a DC glow discharge dusty plasma device. The waves are very likely driven by an ion-dust streaming instability. A generic feature of these waves is their non-sinusoidal waveforms having sharply peaked wave crests and flat wave troughs. This characteristic could be accounted for, qualitatively, in terms of a second-order wave theory. By extending the analysis to second order, an inhomogeneous wave equation was obtained whose solution contained a sum of first and second harmonic waves that provided a reasonable fit to the measured waveforms. Carrying out the perturbation analysis to second order led, not only to quantitative corrections to the first order quantities, but added new effects not accounted for in a linear wave analysis. Second-order wave theories are often used to model large amplitude deep ocean waves (Stokes' waves) [35] and nonlinear sound waves [36].

(2) A slit placed in front of the anode of the DC discharge device was used to create a converging-diverging nozzle configuration that produced large amplitude dust acoustic waves that evolved into dust acoustic shocks. Steepening of the dust acoustic perturbations was observed as the pulses propagated downstream. The shocks developed into nearly time-stationary structures with a thickness approaching the interparticle spacing. The observed shock characteristics were compared to numerical shock solutions of the fully non-linear generalized dust hydrodynamic equations for arbitrary amplitude perturbations. This model included strong coupling effects, dust-neutral collisions, and bulk and shear viscosities. The model calculations agreed remarkably well with the experimental observations.

(3) Structurization of a dust cloud was observed when the dusty plasma was operated at much higher plasma densities than in either experiments (1) or (2) above. When the plasma density was increased beyond a critical point, a significant change in the topology of the dust cloud occurred. A spontaneous transition from propagating dust acoustic waves to non-propagating, stable, spatially periodic dust density structures was observed. This phenomenon was discussed in terms of two instability mechanisms, one based on ionization and ion drag forces and the other on the polarization force, both predicting the growth of non-propagating, growing dust density perturbations.

As pointed out in the introduction, it has been nearly 25 years since Padma Shukla first predicted the existence of the dust acoustic wave. This has inspired an enormous amount of subsequent theoretical work as well as many experimental studies of this fundamental dusty plasma wave. Several papers continue to appear each month reporting on various aspects of the dust acoustic wave.

In January 2013, NASA plans to launch the LADEE (Lunar Atmosphere and Dust Environment Explorer) mission to the moon [37]. One of the purposes of this mission is to study the nature of the dust lofted above the lunar surface and reported by the Apollo astronauts as “moon clouds” [38]. It is conceivable that dust acoustic waves could be observed, in situ, in the moon clouds.

The continued interest in the dust acoustic wave is due in part to the ease with which it can be excited and studied in the laboratory. From a fundamental point of view, however, the dust acoustic waves and shocks may be important as a possible mechanism for triggering dust grain condensation and structurization in planet and star formation regions.

Acknowledgements

The authors are grateful to P. K. Shukla and B. Eliasson for allowing us to use their numerical results on dust acoustic shock waves, and for very useful discussions. This work was supported by DOE Grant No. DE-FG01-04ER54795 and NSF Grant No. PHY-0923141.

References

[1] Shukla P K and Eliasson B 2009 *Rev. Mod. Phys*. **81**, 25

[2] Morfill G E and Ivlev A V 2009 Rev. Mod. Phys. **81**, 1353

[3] Merlino R L and Goree J 2004 *Physics Today* July Issue, 32-38

[4] Rao N N, Shukla P K, and Yu M Y 1990 *Planet. Space Sci*. **38**, 543-546

[5] Shukla P K and Mamun A A 2002 *Introduction to Dusty Plasma Physics* (Bristol: Institute of Physics Publishing)
Vladimirov S V, Ostrikov K, and Samarian A A 2005 *Physics and Applications of Complex Plasmas* (London: Imperial College Press)
Fortov V E and Morfill G E 2010 *Complex and Dusty Plasmas* (Boca Raton: CRC Press)

[6] Morfill G E et al. 2002 AIP *Conference Proceedings* **649** 91-109

[7] Barkan A, Merlino R L, and N. D'Angelo N 1995 *Phys. Plasmas* **2**, 3563

[8] Rosenberg M 1993 *Planet. Space Sci.* **41**, 229

[9] Merlino R L 2009 *Phys. Plasmas* **16**, 124501

[10] Flannigan T M and Goree J 2010 *Phys. Plasmas* **17**, 123702

[11] Heinrich J R, Kim S H, Meyer J K, and Merlino R L 2011 *Phys. Plasmas* **18**, 113706

[12] Thompson C, Barkan A, D'Angelo and Merlino R L 1997 *Phys. Plasmas* **4**, 2331-2335

[13] Bouchoule A and Boufendi L 1993 *Plasma Sources Sci. Technol.* **2** 204

[14] Xu W, Song B, Merlino R L, and D'Angelo N 1992 *Rev. Sci. Instrum*. 63, 5266-5269

[15] Trottenberg T, Block D, and Piel A 2006 *Phys. Plasmas* **13**, 042105

[16] See, e.g., 2011 *Planetary and Space Science* **59,** number 14, which is devoted entirely to lunar dust

[17] Ikezi H 1986 *Phys. Fluids* **29**, 1764

[18] Merlino R L, Heinrich J, Kim S H, Meyer J K 2012 *Phys. Plasmas* 19, 057301

[19] Merlino R L 2012 Physica Scripta 85, 035506

[20] Montgomery D 1967 *Phys. Rev. Lett.* **19**, 1465

[21] Spitzer L 1978 *Physical Processes in the Interstellar Medium* (New York: Wiley Interscience)

[22] Popel S I and Tsytovich V N 1999 *Astro. Space Sci.* **264**, 219

[23] Samsonov D, et al. 2003 *Phys. Rev. E* **67** 036404

[24] Whitham G B 1974 Linear and Nonlinear Waves (New York: Wiley Interscience)

[25] Heinrich J R, Kim S H, and Merlino R L 2009 *Phys. Rev. Lett.* 103, 115002

[26] Shukla P K and Eliasson B 2012 *arXiv*:1205.5947v2, submitted to *Phys. Rev. Lett*.

[27] Gupta M R, Sarkar S, Ghosh S, Debnath M, and Khan M 2001 *Phys. Rev. E* **63**, 046406

[28] Gollub J and Langer L 1999 *Rev. Mod. Phys.* **71**, S396

[29] Morfill G and Tsytovich V 2000 *Plasma Phys. Rep*. **26**, 682

[30] Pandey B P, Avinash K, and Dwivedi C B 1994 *Phys. Rev. E* **49**, 5599
see also, Verheest F 2000 *Waves in Dusty Space Plasmas* (Dordrecht: Kluver Academic Publishers)

[31] Heinrich J R, Kim S H, and Merlino R L 2011 *Phys. Rev. E* **84**, 026403

[32] D'Angelo N 1998 *Phys. Plasmas* **5**, 3155

[33] Khrapak S A, Ivlev A V, Yaroshenko V V, and Morfill G E 2009 *Phys. Rev. Lett.* **102**, 245004

[34] Hamaguchi S and Farouki R T 1994 *Phys. Rev. E* **49**, 4430

[35] Dean R G and Dalrymple R A 2001 *Water Wave Mechanics for Engineer and Scientists*, (Singapore: World Scientific Publishing Co. Pte. Ltd.)

[36] Morse P K and Ingard U 1968 *Theoretical Acoustics,* (New York: McGraw-Hill)

[37] see, http://www.nasa.gov/mission_pages/LADEE/main/

[38] Rennilson J J and Criswell D R 1974 *The Moon* 10 121-142

TABLE 1 Plasma and dust parameters of the experiments

Parameter	**Value**	**Comments/Measurement**
Plasma parameters		
ion density, n_i	10^{14} –10^{15} m^{-3}	double probe
electron temperature, T_e	2 – 3 eV	double probe
ion temperature, T_i	0.025 eV	same as neutrals
axial electric field	150 – 300 V/m	emissive probe
neutral gas	argon	
neutral pressure	100 – 200 mtorr	Baratron gauge
magnetic field	3 – 5 mT	Hall probe
Dust parameters		
charge, Q_d	(2000 – 10,000)e	OML theory
number density, n_d	10^{10} – 10^{11} m^{-3}	video imaging
dust composition	size (diameter)	type
kaolin powder	1 – 5 μm	various shapes/sizes
hollow glass spheres	< 30 μm	polydisperse
silica spheres	1 μm ± 0.2 μm	monodisperse
iron spheres	1 – 4 μm	polydisperse

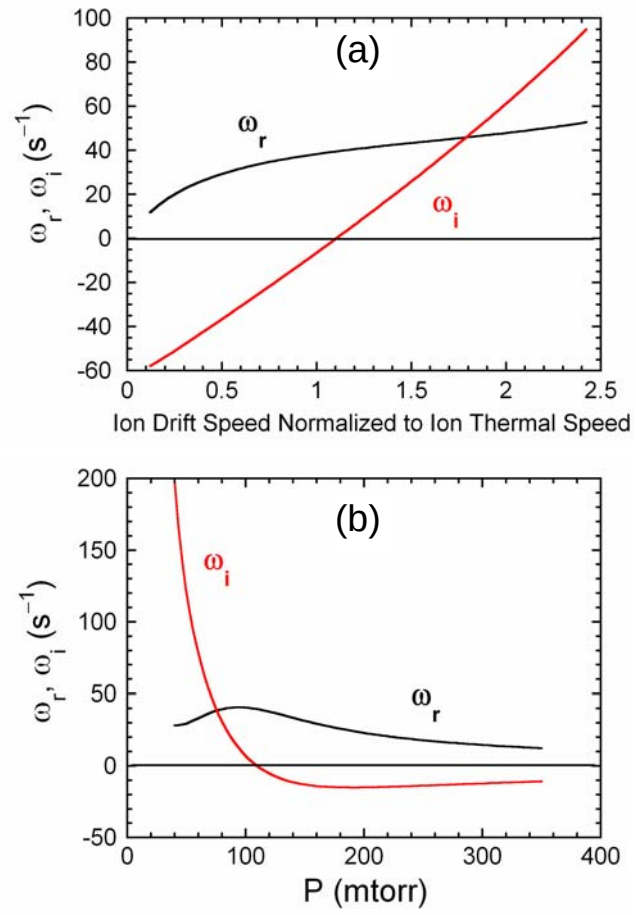

FIGURE 1. Numerical solution of the fluid dispersion relation for the ion-dust streaming instability. (a) Real and imaginary parts of the dispersion relation vs. ion drift speed normalized to the ion thermal speed. (b) Real and imaginary parts of the dispersion relation vs. neutral pressure.

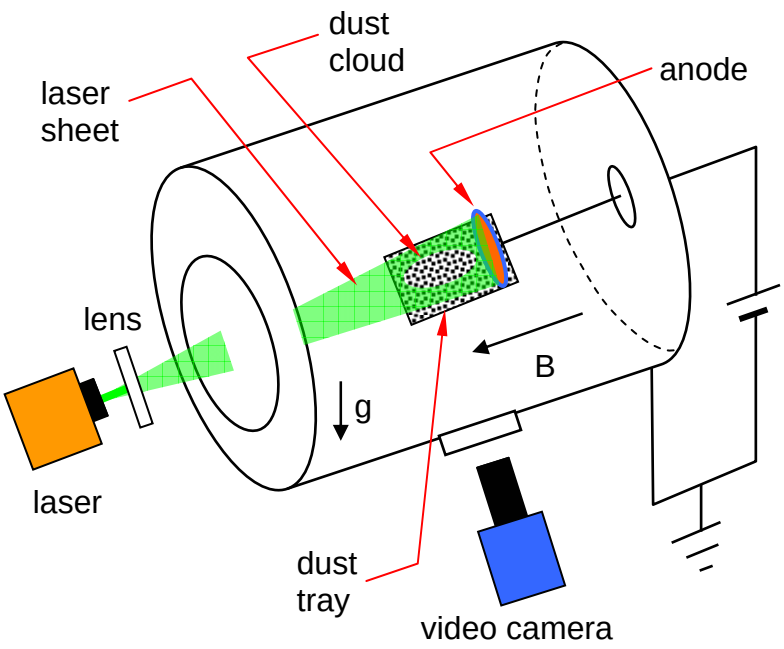

FIGURE 2. Schematic of the experimental set-up. The plasma is formed by a glow discharge in argon between a 3.2 cm anode disk and the grounded walls of the vacuum chamber. A magnetic field of ~ 3 mT produced by 6 water-cooled coils (not shown) is used to confine the electrons. The dust is introduced into the plasma from a tray below the anode. The dust is illuminated with a thin sheet of 532 nm laser light and imaged on a fast video camera.

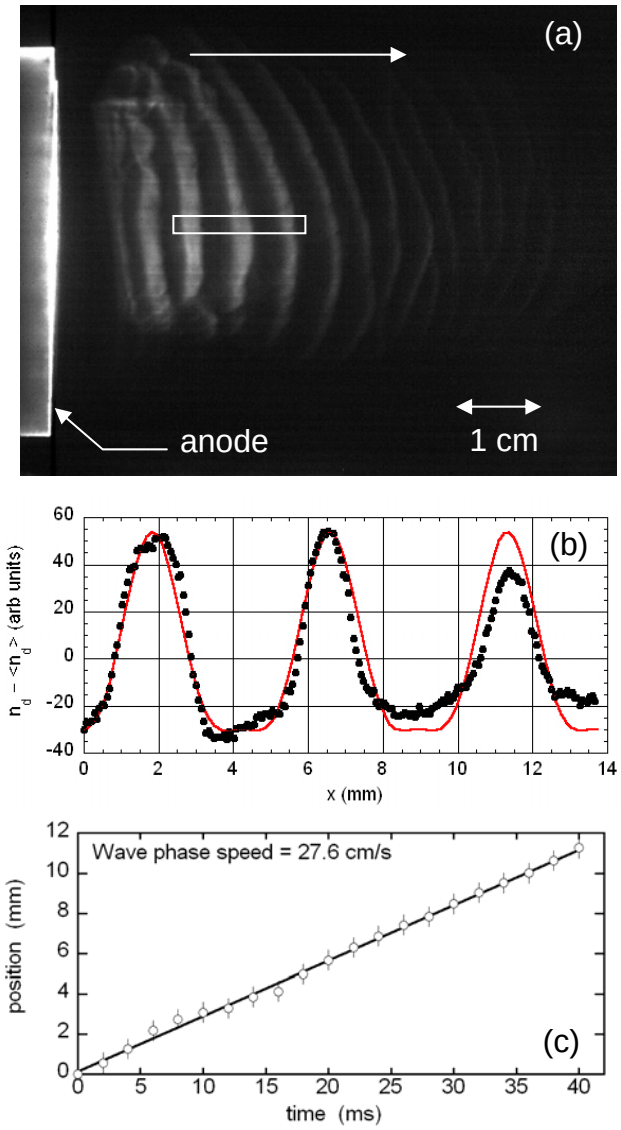

FIGURE 3. Nonlinear dust acoustic waves. (a) Single frame video image of a large amplitude dust acoustic wave propagating away from the anode (in the direction of the ion drift). (b) Solid circles: Experimental values of the dust acoustic waveform corresponding to the rectangular box in (a). Solid line: Theoretical waveform fit obtained from equation (12). (c) Position of one wavefront vs. time obtained from the video recording of the dust acoustic wave.

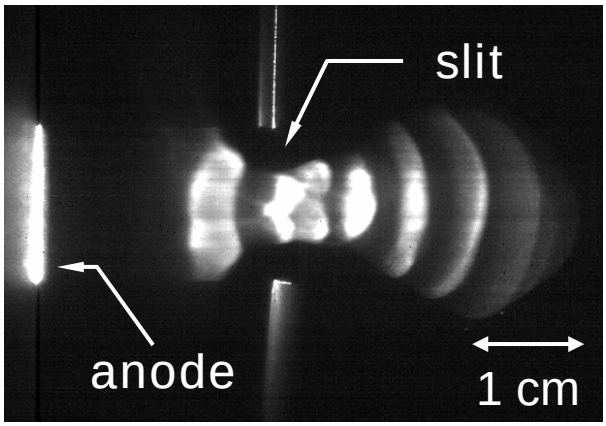

FIGURE 4. Single frame video image of the set-up used to produce dust acoustic shock waves. A 1 cm wide electrically floating slit is placed in front of the anode to produce a converging/diverging potential contour configuration. Dust acoustic waves produced on the anode side of the slit are compressed while propagating through the slit, and evolve into dust acoustic shocks.

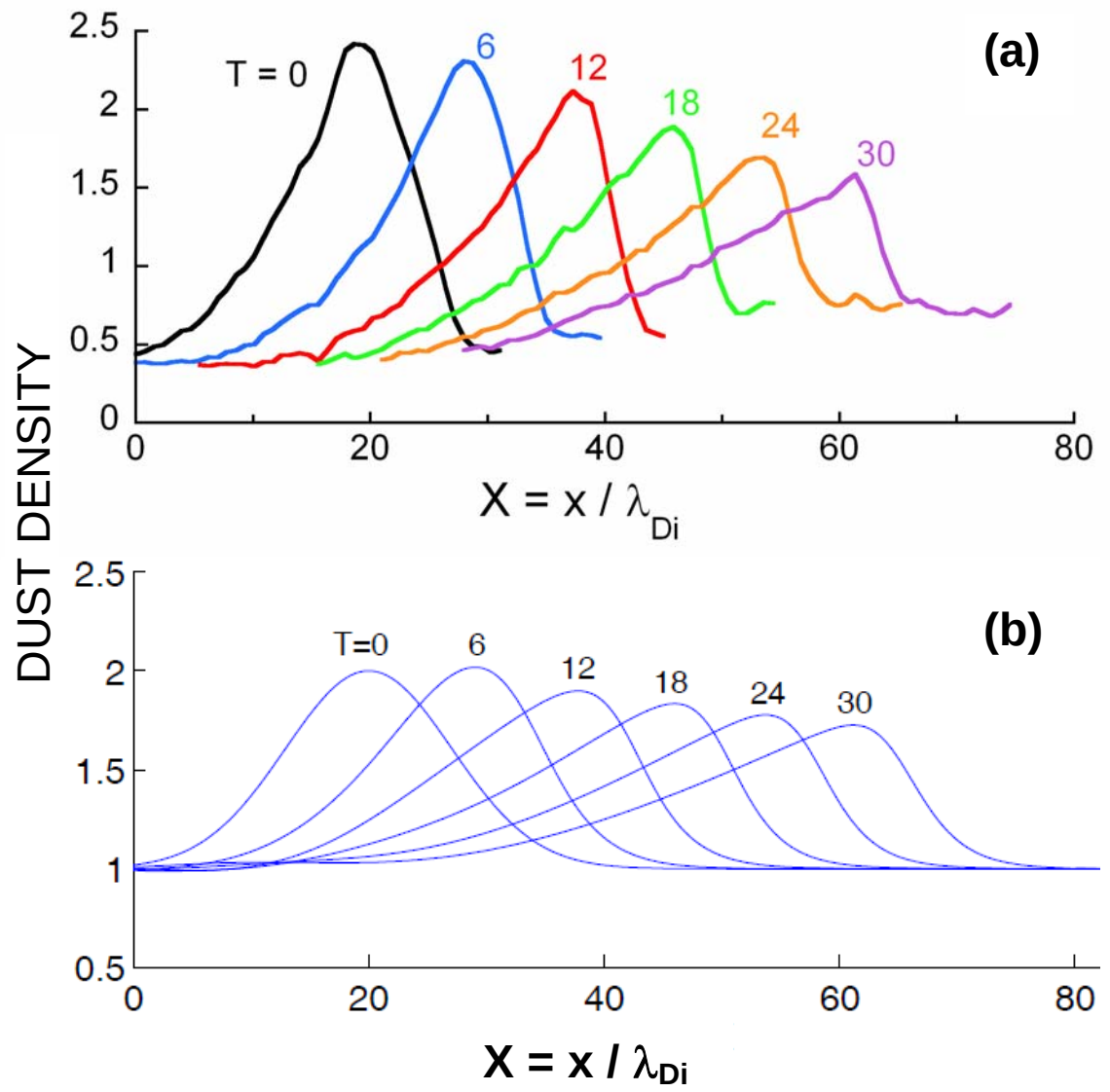

FIGURE 5. Dust acoustic shock waves. (a) Evolution of a dust acoustic shock wave. Times are normalized with the dust plasma frequency. Steepening of the shock is observed as it propagates. (b) Results of a numerical calculation of the formation of large amplitude dust acoustic shocks using the theoretical model described in Ref. 26.

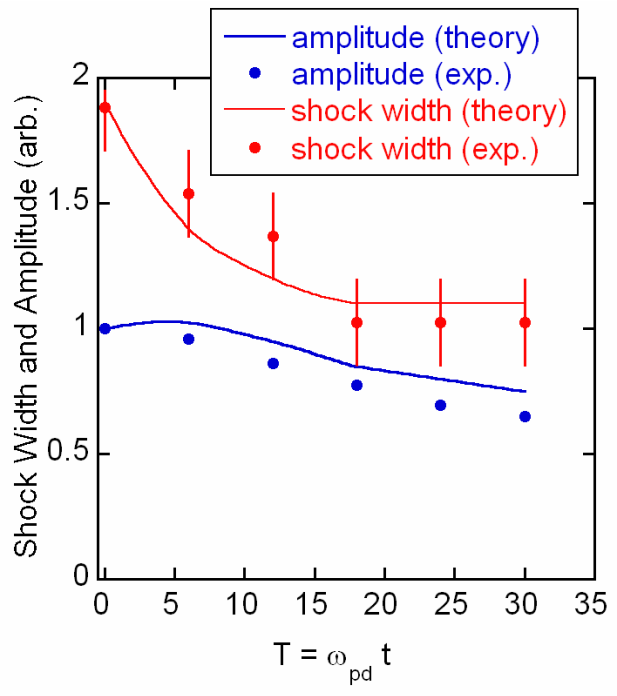

FIGURE 6. Solid circles: Shock amplitude and width obtained from the data shown in Fig. 5 (a). Solid lines: theoretical shock amplitude and width obtained from the results shown in Fig. 5 (b), normalized to experimental values at T=0.

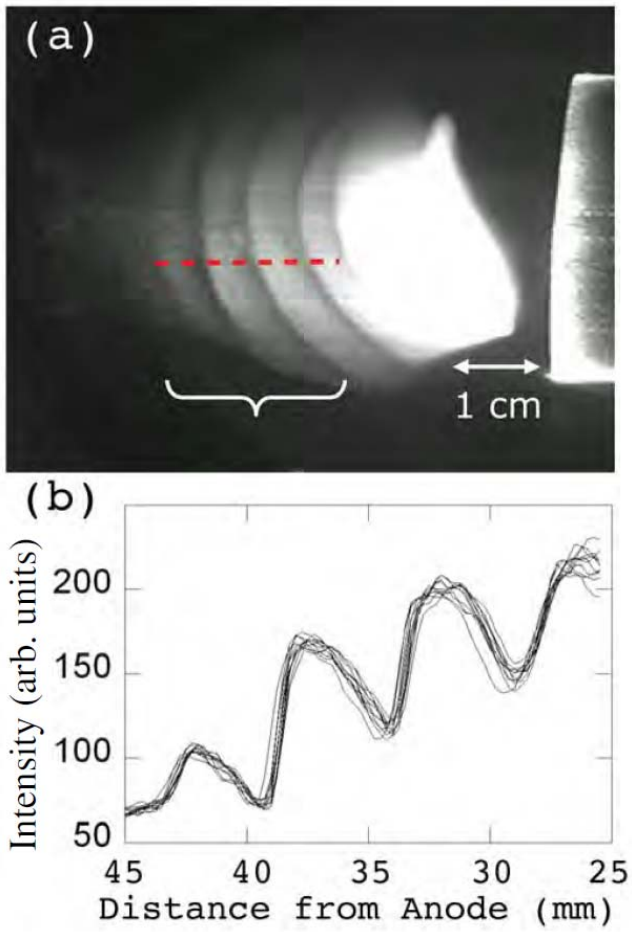

FIGURE 7. Dusty plasma structurization. (a) Single frame video image of a structured dust cloud with stationary and stable regions of high and low dust density. (b) Profile of the dust density taken across the dashed line in (a). Multiple profiles recorded over a 33 s period are overlaid to show that the structures are stationary.

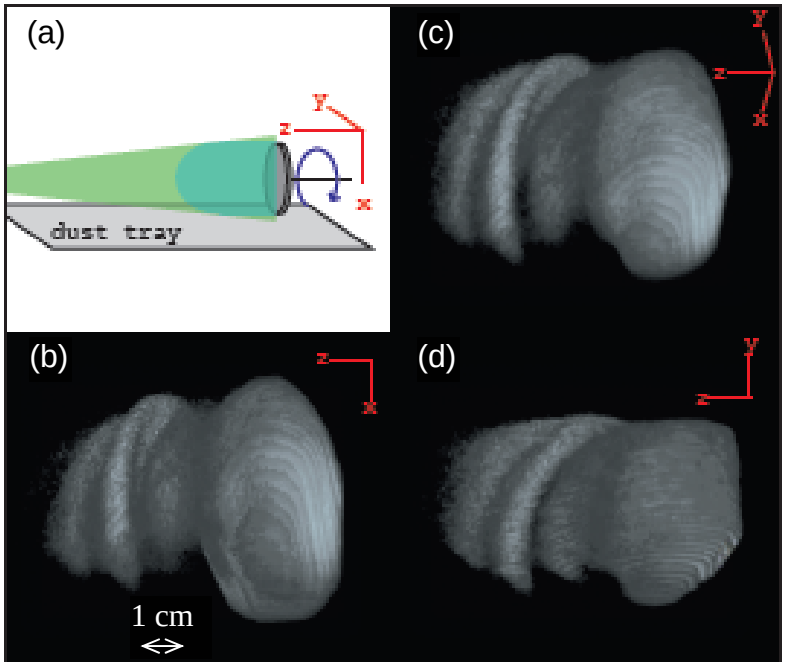

FIGURE 8. Tomographic reconstruction of the structured dust cloud. The axis orientation is shown in (a). The cloud is illuminated by a laser sheet in the x-z plane. 3D views are shown in (b), (c), and (d) as the point of view is rotated (in the direction of the blue arrow in (a). The tomographic reconstruction shows the nonplanar nested conical shell structure of the zero-frequency dust density striations. The anode was removed in the images to improve clarity.